



**HAL**  
open science

## An application of speckle-based background oriented schlieren for optical microcalorimetry

Quentin Michalski, Julien Sotton, Alain Claverie, Marc Bellenoue

► **To cite this version:**

Quentin Michalski, Julien Sotton, Alain Claverie, Marc Bellenoue. An application of speckle-based background oriented schlieren for optical microcalorimetry. 18th International Symposium on the Application of Laser and Imaging Techniques to Fluid Mechanics, Jul 2016, Lisbon, Portugal. hal-01468085

**HAL Id: hal-01468085**

**<https://hal.science/hal-01468085>**

Submitted on 15 Feb 2017

**HAL** is a multi-disciplinary open access archive for the deposit and dissemination of scientific research documents, whether they are published or not. The documents may come from teaching and research institutions in France or abroad, or from public or private research centers.

L'archive ouverte pluridisciplinaire **HAL**, est destinée au dépôt et à la diffusion de documents scientifiques de niveau recherche, publiés ou non, émanant des établissements d'enseignement et de recherche français ou étrangers, des laboratoires publics ou privés.

# An application of speckle-based background oriented schlieren for optical microcalorimetry

Quentin Michalski\*, Julien Sotton, Alain Claverie, Marc Bellenoue  
Institut Pprime, (CNRS, UPR 3346, Université de Poitiers, ENSMA)  
1 Av Clément Ader, Téléport 2, BP 40109, 86961 Futuroscope Chasseneuil, France  
\* Correspondent author: quentin.michalski@ensma.fr

**Keywords:** Background Oriented Schlieren, Calorimetry, Spark, Ignition

## ABSTRACT

The aim of the present study is to validate an experimental method of in-fluid enthalpy variation measurement by means of Speckle-based Background Oriented Schlieren (SBOS). The method applies on resolving the millijoule thermal-energy transfer to fluid induced by an electric discharge in air. Intensified camera is used to match the electric discharge exposure time constraint. Speckle is used as the reference pattern as it allows an easier access to high density pattern for subcentimetric imaging. Geometric optics principles are used to extract line of sight integrated index of refraction. Local density field is then computed through filtered back projection of Gladstone-Dale equation. The method is first validated in close experimental conditions provided by the density measurement of a millimeter-dimensions CO<sub>2</sub> gaseous laminar jet. An analysis on the jet gives useful insights on noise sources and uncertainties of the method which is then transposed to the discharge. Results of enthalpy measurements are discussed.

---

## 1. Introduction

Ignition and flame stabilization in combustible mixtures are among the most challenging problems in fundamental and applied combustion research (Glassman and Yetter 2008). In particular, control of ignition in helicopter engines is a key point to achieve better performances. As an example, capability of a quick engine relight in case of a flameout at high altitudes and low combustor pressures is extremely desirable.

The first step in the ignition process is creation of a small-size flame kernel by the ignitor. Initial behaviors of this flame kernel depend on the energy release to the flow by the ignition system. For this purpose, new ignition concepts are studied using laser ignition (Tauer, Kofler and Wintner 2010), corona discharge ignition (Bellenoue and al. 2007), radiofrequency ignition, nanosecond repetitive pulse discharge (Grish and al. 2011) (Pancheshnyi and al. 2006) (Xu 2013). Some of them are still based on electrical discharges. Then energy released to the flow and electrical consumption must be determined in order to be able to really compare efficiency of such ignition system. Several methodologies are developed to quantify the thermal energy release to the flow like

microcalorimetry (Teets and Sell 1989), CARS diagnostics (Grisch and al. 2011), Raman spectroscopy, LIF, etc.

Methodology described in the paper is the use of a quantitative Background Oriented Schlieren (BOS) (G. Meier 1999) (Dalziel, Hughes and Sutherland 1998). BOS is based on the refractive index variation of fluid due to density gradients. Variations of refractive index due to density gradient have been qualitatively used for a long time to perform visualizations, like shadowgraphy or schlieren, in compressible flow or reactive case.

Principles of implementation of the method are quite simple, as it only requires a single camera, a static structured background and a computer for processing. Images are taken with and without optical distortion. A numerical comparison of both images is done using cross-correlation algorithms and gives out the integrated displacement vector which then, through further calculation yields other physicals according to the measured medium properties.

On a quantitative level, numerous works illustrate BOS rendering capabilities and emphasize BOS qualitative measurement qualities as it provides a wide adaptable sensibility range and acquisition field size. BOS has been applied to most conventional schlieren case of application, as several studies shows. Quantitative measurement can also be achieved and physical field measurement of density (Elsinga and al. 2004) (Hargather and Settles 2012) (Meier and Venkatakrisnan 2004) (Ota, Hamada and Maeno 2010) and temperature in reactive fluids (Iffa, Aziz and Malik 2011) has been achieved. Elsinga (Elsinga and al. 2004) and Hargather (Hargather and Settles 2012) works provide comparisons between BOS and other quantitative schlieren methods, with respectively calibrated colored schlieren and calibrated schlieren, and shows results within 2-3% of theory which sets BOS quantitative capabilities.

Recently, Meier (Meier and Roesgen 2013) proposed using the speckle of a laser as a background (SBOS). SBOS allows for fine dynamic tuning over background spatial resolution even at high optical magnification.

The objective here is first to achieve a quantitative measurement of the density and assess the temperature distribution in the electric discharge kernel. The integration of the temperature field over the kernel then yields a quantitative enthalpy measurement. The method is first applied on the analysis of a laminar low Reynolds  $\text{CO}_2$  jet. It provides results which allows for uncertainty and noise investigation of the method which is then applied to electric discharges where enthalpy measurement is performed.

## 2. Method

### 2.1. Optical configuration and signal origin

In this section we introduce the optical concepts and hypothesis that link the integrated refraction index to the measured displacement field. The optical configuration is similar to the one described in Meier (Meier and Roesgen 2013).

Schlieren method is based on the principle that when propagating through optically heterogeneous medium, the light ray trajectory bends according to refractive index gradient. Such a behavior is mathematically modeled by the eikonal equation. If one suppose the z-axis of a right-handed Cartesian  $x,y,z$  coordinate system being the direction vector of the undisturbed light ray, the eikonal equation yields the resulting curvature which is then given by

$$\begin{cases} \frac{\partial^2 x}{\partial z^2} = \frac{1}{n} \frac{\partial n}{\partial x} \\ \frac{\partial^2 y}{\partial z^2} = \frac{1}{n} \frac{\partial n}{\partial y} \end{cases} \quad (1)$$

One can integrate those equations along the light path  $\mathcal{C}$  which yield the schlieren intrinsic angular ray deflection  $\varepsilon$  and its components along  $x$  and  $y$ ,

$$\begin{cases} \varepsilon_x = \frac{1}{n} \int_{\mathcal{C}} \frac{\partial n}{\partial x} dz \\ \varepsilon_y = \frac{1}{n} \int_{\mathcal{C}} \frac{\partial n}{\partial y} dz \end{cases} \quad (2)$$

Doing so, one should keep in mind that because  $\varepsilon$  results from integrating a gradient, the local measurement obtained at the end should only be a refractive index variation. One can estimate the expected maximum intensity of  $\varepsilon$  based on the deviation that would occurred at the extremity of a gas sphere of refractive index  $n$  placed in a fluid of refractive index  $n_0$  based on Keagy's (Keagy, Ellis and Reid 1949) calculations. It roughly gives

$$\varepsilon_{max} \sim 2(n/n_0 - 1) \quad (3)$$

Usually refractive index is not the measure of interest. In fluids, the Lorentz-Lorenz equation states a relation between refractive index  $n$  and density  $\rho$  which can be simplified as the known Gladstone-Dale equation

$$n - 1 = \rho G \quad (4)$$

$G$  is the Gladstone-Dale constant which can be found in tables or calculated based on refractive index measurement and volumic mass calculation in the respective conditions. The same variation on  $n$  is thus observed on  $G$  which depends mainly on both the fluid composition and the wavelength used. In BOS configuration, the angular intrinsic deflection is materialized on a screen through a mirage effect which is a function of the optical collection configuration and efficiency (Fig. 1).

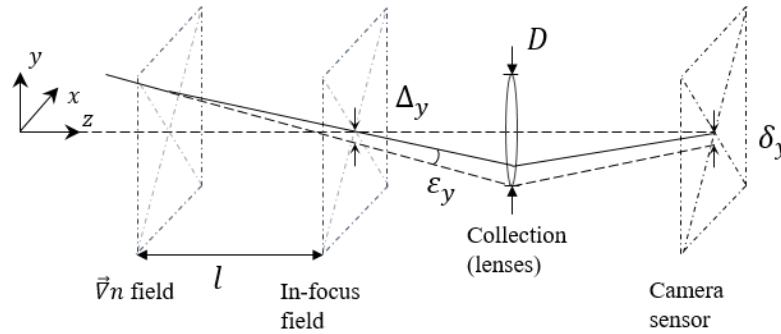


**Fig. 1:** Geometry of BOS configuration with negative focus to subject field distance

Simple geometrical considerations based on Fig. 1, assuming optical Gaussian conditions and near axes ray light yields expression of the integrated displacement field  $\delta$  as

$$\vec{\delta} = lM\vec{\varepsilon} \quad (5)$$

Where  $M$  is the optical magnification of the optical system (i.e. the magnification measured in the in-focus field) and  $l$  the « defocusing » distance.  $A = lM$  can be considered as the optical amplification constant. Most published works have so far used Eq. (5). One should notice that doing so, one makes the hypothesis that the distortion happens in one unique refraction plan therefore that the radius of the schlieren object  $w$  is negligible compared to the defocusing distance. The recent work of van Hinsberg & Rösger (van Hinsberg and Rösger 2014) emphasize the importance of this hypothesis and shows that the error ratio between the measured, under the precedent hypothesis, angular deviation  $\varepsilon$  and the real deviation  $\varepsilon_{th}$  can be estimated by

$$(\varepsilon_{th} - \varepsilon)/\varepsilon = w/l \quad (6)$$

When considering microscopic application or simply when increasing the spatial resolution of any BOS system,  $M$  should increase. At a constant  $A$ , it implies that  $l$  should decrease which then results in a loss of accuracy because of an increasing  $\varepsilon/\varepsilon_{th}$  error ratio. As seen on most BOS picture the in-



## 2.2. Speckle-based Background Oriented Schlieren

Implementation of BOS is quite simple as it technically only requires a background and a camera to work. On a first approach, one should notice that because cross-correlation algorithm from PIV applications are used to determine displacement, therefore any background looking like a PIV-seeded flow will give good results for BOS. For qualitative and visualization purposes, it is easily evidenced that any background with enough contrast will work for the algorithm. Several backgrounds have been used to obtain quantitative measurement on density, such as dot printed black and white ones (Elsinga and al. 2004), printed black and white wavelet noise (Iffa, Aziz and Malik 2011) or regular colored grid (CGBOS (Ota, Hamada and Maeno 2010)). More recently the work of Meier (Meier and Roesgen 2013) introduces the speckle of a laser as a background choice. Speckle photography already used likewise configurations (Fomin 1998) except that computation capacity and algorithm as well were not in place at the time it was considered. Eq. (5) still stands in speckle configuration, furthermore this time, speckle being observed in the focal plan, one can work with negative value of defocusing distance. According to Meier (Meier and Roesgen 2013) compared to an equal but positive sign distance, working with negative distance greatly increases sensitivity. Such configuration proves to considerably reduce the distance needed to achieve equivalent sensitivity with positive distance.

Speckle patterns are of interferential nature and are formed when scattered, i.e. therefore spatially randomly phased, coherent light interfer on a sensor surface. It can be shown (Fomin 1998) that when collecting the speckle through an optic system, the speckle dot mean « diameter », i.e. characteristic size,  $\Delta_s$  is such as

$$\Delta_s \approx 1.22\lambda N \frac{1+M}{M} \quad (8)$$

Where  $\lambda$  is the wavelength of the coherent light. As of Eq. (8),  $\Delta_s$  varies in regard of the collection system exit pupil diameter which is easily experimentally verified. PIV software criteria advises using dots of 2-5 pixel/dots to achieve optimum spatial resolution, then when looking at investigating small dimension, printing resolution can become an issue (looking at more than 1200dpi). When working with speckle this problem is overcome by increasing the diaphragm opening which indeed may result in a loss of gradient resolution given equation (7).

### 3. Experiments

#### 3.1. Reference flow configuration and motivations

Our objective is to achieve a small enthalpy variation measurement in electrical discharges kernel by SBOS through refractive index measurement. In order to validate the SBOS configuration we ought to find a suitable configuration close in dimension and  $\varepsilon$  to discharge kernel conditions. Discharge energy transfer efficiency and kernel dimensions found in literature (Maly 1984) considering an energy deposit of 40mJ, under hypothesis for the kernel gas we extensively discuss in following sections and using Eq. (3) it yields  $\varepsilon_{max} \sim 3.4 \cdot 10^{-4}$  which is relatively close in magnitude to  $\text{CO}_2$  observed in air at ambient conditions  $\varepsilon_{max, \text{CO}_2} \sim 3 \cdot 10^{-4} \text{rad}$ . Although the difference of density gradient direction may affect the overall physic of each phenomenon, following Eq. (5), the only noticeable difference, from the method perspective should only be in the displacement direction and should not affect the measurement. The validation is thus made on the resolution of density of a  $\text{CO}_2$  laminar jet.

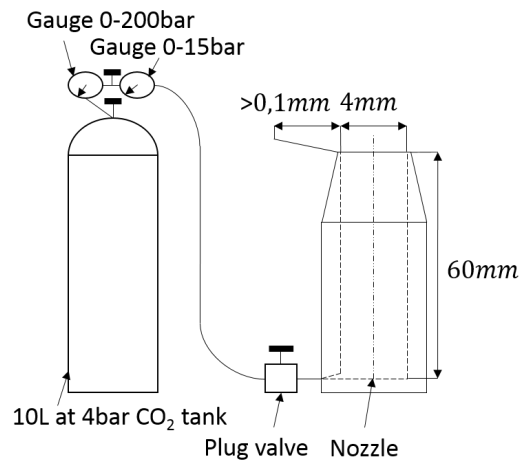


Fig. 3: Schema of flow configuration

The gas is supplied by a 4bar, 10L  $\text{CO}_2$  pressure tank (gas impurities  $<50\text{ppm}$ ), the nozzle inside diameter is of 4mm and consist of a machined 6x4mm tube at a  $11.5^\circ$  angle. To ensure ideal steady flow conditions, the 4mm diameter is reamed on 60mm long. Estimations based on upstream pressure yields a Reynolds number, calculated with nozzle diameter, low enough (estimated to be around 40) to ensures laminar flow in steady conditions. Pressure expansion is low enough to suppose that  $\text{CO}_2$  temperature variation is negligible. As BOS measurement only gives a differential density measurement, ambient temperature is measured in the room,  $T_0 = 20.0 \pm 0.5^\circ\text{C}$  and pressure is supposed to be  $p_0 = 1.00 \pm 0.01\text{bar}$  which yields  $\rho_{\text{CO}_2} = 1.806\text{kg}/\text{m}^3$  and  $\rho_{\text{air}} = 1.190\text{kg}/\text{m}^3$ .

### 3.2. Optical configuration

The coherent source is a diode-pumped continuous solid-state laser (MxL-F,  $\lambda = 532nm$ , 3W) which emission power is stabilized in steady conditions at 1%. The beam is expanded through a collimator. Parallel beams expanded to a 45mm diameter impact a 1mm width ground glass which produces the speckle by scattering effects (Fig. 4).

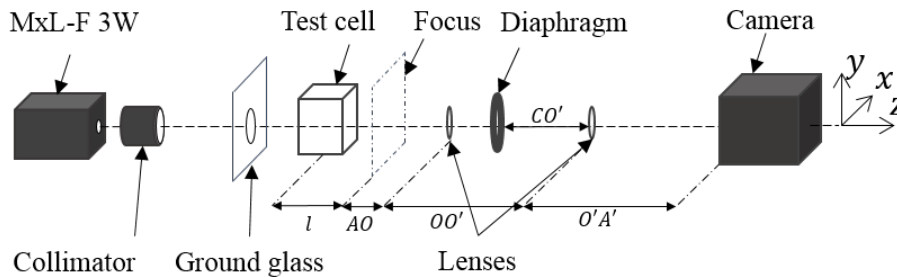
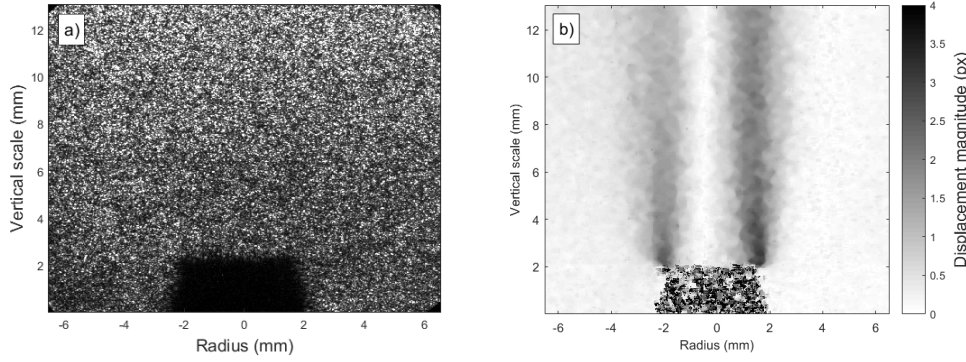


Fig. 4: Schema of optical configuration

Our optical collection system consists of two lenses, of focal length and center respectively  $O$  and  $f_1 = 500mm$  and  $O'$  and  $f_2 = 300mm$ , and of a diaphragm, focus the speckle light on the naked camera sensor plan. The camera used is a PiMax 1k GenII RB-SG, CCD intensified camera with a 1Hz acquisition which suits the need for the short exposure time required. Intensification is channeled using fiber optic coupling which greatly reduces loss of resolution and distortion. Under laminar conditions, close to the nozzle, flow is supposed to be axisymmetric enough to consider a single view for tomography. Pixel size is  $c = 13\mu m$ . Optimum quality/exposure time ratio has been found using a 250 (on a maximum of 255) intensifier gain value, and 65% of the maximum laser power (as to avoid photocathode damaging during long acquisition). Although the whole discharge process takes about 2.5ms, rapid advection movement occurs therefore the exposure time is chosen as short as possible. The best trade-off, imaging-wise, is found for  $1\mu s$  exposure time which is thus also used for the  $CO_2$  jet. The lenses positioning was  $AO = 170mm$ ,  $OO' = 492mm$  and  $OA' = 500mm$  which ensures a global magnification ratio of  $M = -1.0$ . The diaphragm positioned at C, is closed at 5mm in diameter which, at a distance  $CO' = 45mm$ , yields an effective exit pupil diameter of  $D \sim 5,32mm$ . This configuration yields a speckle size of  $61.6\mu m$  which is about 4.7px which fits PIV software requirements. The defocusing distance is  $l = -80mm$



**Fig. 5:** Exemple of reference image under no-flow condition (a) and mean displacement magnitude field in pixel (b), in each case radius is the distance from the center of the nozzle.

Fig. 5 gives a quantitative idea of the overall image acquisition quality (Fig. 5a) obtained under no flow conditions and the mean displacement intensity (Fig. 5b) of the CO<sub>2</sub> flow. The nozzle edge, at the bottom of the image, appears blurry and the speckle which constitutes the background, remains sharp as expected.

#### 4. BOS processing

The acquisition is made on 100 images at a 0.2Hz camera frequency, the same reference image is being used for each of them. The CO<sub>2</sub> jet acquisitions are processed with MatPIV (Sveen 2004). Given a maximum displacement  $\delta_{max} = 3px$ , the MatPIV multipass interrogation windows starting at 32x32 and finishing at 16x16 is used with a 87.5% overlap. Based on the final interrogation window size the spatial resolution achieved is  $\Delta x = 0.208mm$ . An important overlapping is used, which may not be an optimum, but prevents discretization issues in onwards gradient integrations. Overlapping does not yield truly independent vectors (Raffel, Willert and Kompenhans 1998), which even if they aren't proper individual measurements at least act as relevant and precise interpolations. Images of 1024x1024px yields a field of 505x505 vectors. A mean displacement field is then computed. Displacements field must then be integrated. Therefore two possibilities exists, one can solve the tomography problem, obtain the gradient field which is then integrated. The other way is to notice that because the derivation is orthogonal to the integration, one can first integrate, then solve the tomography problem. In respect of Leibniz integral rule, Eq. (2) coupled to Eqs. (4) and (5), then yields the following system to integrate

$$\begin{cases} \frac{n_0 \delta_x}{GMI} = \frac{\partial}{\partial x} \int_C \rho(x, y, z) dz \\ \frac{n_0 \delta_y}{GMI} = \frac{\partial}{\partial y} \int_C \rho(x, y, z) dz \end{cases} \quad (9)$$

Gladstone Dale constant is set from tables (Fomin 1998) with  $G = 0.229\text{cm}^3/\text{g}$  and refractive ambient air index is taken at  $20^\circ\text{C}$  and  $p = 1\text{bar}$ ,  $n_0 = 1.00027$ . Differentiation and sum of (9) system's equations yields the Poisson equation which is classically solved in BOS. A rather quicker way to solve this system is to directly integrate the displacement line by line which induces a lot less smoothing than the elliptical solution. Integration is performed along the direction which present best signal to noise ratio. The line of sight integrated density (projection) is then processed through the inverse Radon transform where the usual Ram-Lak ramp filter is modulated by an Hamming window. The window filtering greatly attenuates the projection high frequency spatial components which are assumed to be mainly noise related and may therefore be reduced to negligible values without affecting the density distribution (Meier and Venkatakrishnan 2004). Additional filtering by directly truncating high frequency noises (up to the Nyquist) using a reduced windows width was not required.

## 5. Validation results

Flow is estimated to be laminar thus supposed to present relatively stable parallel and axisymmetric conditions at nozzle exit along several diameters. On the jet, one reference image is taken then a hundred acquisitions are made. For each, a displacement field is computed. BOS processing is then applied to the averaged displacement field. Left Fig.6.a shows the density profile in the jet averaged along the axis on a one diameter (4mm) distance from the nozzle tip. As expected, consequences of the reconstruction filtering, the radius density profile are rather smooth and show no high frequencies. The mean difference of density measured at jet core on 4mm long is 2.3% less than expected, which yields a 0.8% error on CO<sub>2</sub> density. The jet sides show gradients spread on a 1.77mm distance, measured for a variation from 10% to 90% of maximum density. This value should be compared to the spatial resolution superior limit calculated from Eq. (7) which yields  $d_{av} = 0.86\text{mm}$ . Right Fig. 6b presents the reconstructed, on 4mm long, jet density at core. Its presents clear stochastic oscillations of 3.5% around the mean value. These oscillations do not disappear after temporal averaging operations thus are not assumed to be related to any oscillating jet instability.

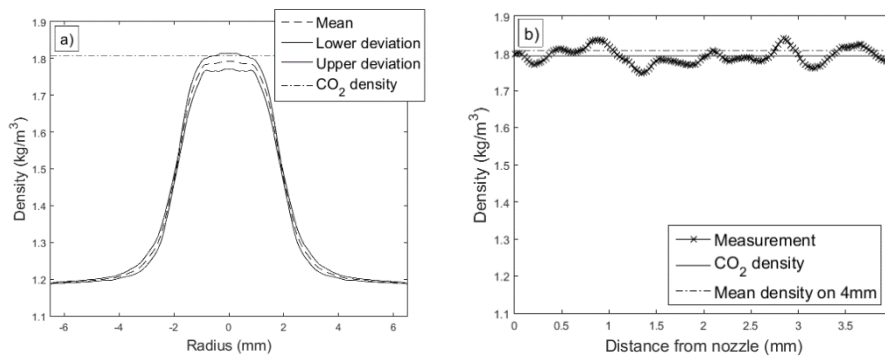


**Fig. 6:** Density distribution shape taken on 4mm above nozzle exit (a) and density in the jet core ( $r=0$ ) (b). Averaging lowers to negligible value any MatPIV induced peak-locking (as noted in (Atcheson, Heidrich and Ihrke 2009)). Fig. 7 shows displacement profiles along a radius at  $y = 1.34\text{mm}$  and  $y = 2.84\text{mm}$  which are the position of the two extremes value of Fig. 6b, which look almost identical. Those profiles present the same medium-high frequency oscillations as observed on the Fig. 6b.

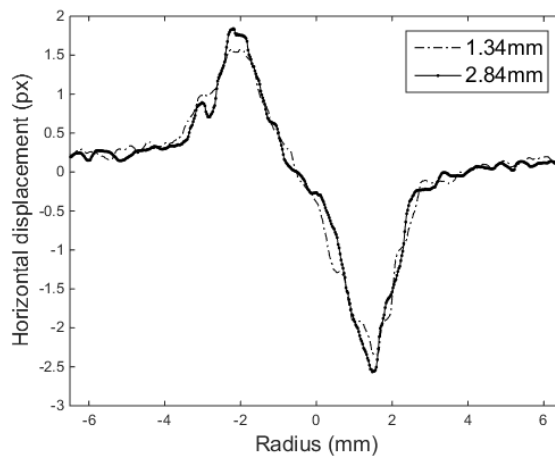


**Fig. 7:** Displacement profiles at extreme Fig. density fluctuation values

In SBOS as in BOS, noises origin from both step of the density field measurement, the acquisition and the reconstruction. During the acquisition, typical BOS noise sources are mainly camera sensor intrinsic noise (i.e. CCD dark current), vibration of the pattern generator (e.g. the ground glass in SBOS or the screen in BOS), local room temperature gradient and intensification noise in our case. Fig. 8 shows the typical remnant noise in reference images cross-correlations which consists in high frequencies (superior to  $4\mu\text{m}$ ) background displacement fluctuation for which part of it can actually be considered as speckle luminous intensity locally waves during acquisition. Reconstruction first step, cross-correlation presents an intrinsic uncertainty which may be considered as a white noise during the reconstruction and may largely account for what is seen on Fig. 8. Vibration effects may introduce a displacement bias which may be compensated. Considering the refractive object axisymmetric, the overall average of the displacement field

should be zero and therefore before reconstruction, the field residual mean displacement is subtracted.

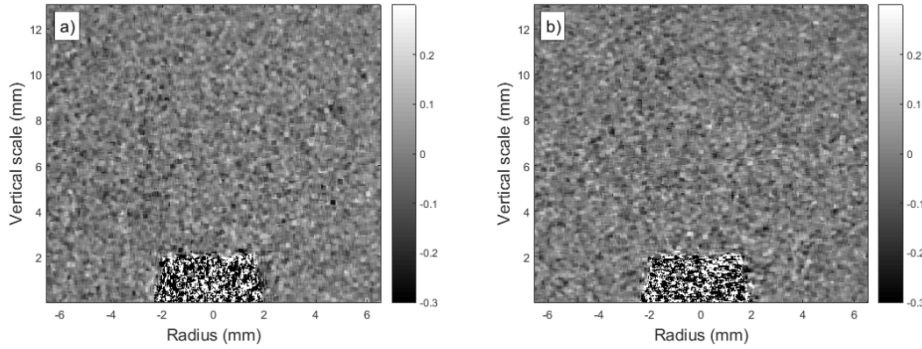


**Fig. 8:** Mean horizontal displacement (a) and displacement RMS (b) in pixels between 10 references images. A first approach on an estimation of the uncertainty on density profile measurement (Fig. 6a.) can be given by applying a logarithmic differentiation on integrated Eq. (9). On  $\delta_x$  it yields

$$\Delta I/I = \Delta n_0/n_0 + \Delta G/G + \Delta M/M + \Delta l/l + J \quad (10)$$

Where  $J$  is the term that accounts for the uncertainty on the integral of the displacement profile and is detailed hereafter. First four terms are easily estimated with the first one being negligible and the uncertainty on the Gladstone-Dale constant too (Bideau-Mehu and al. 1973). The magnification  $M$  measurement is done, measuring an object in the focus plan, knowing its dimension ( $1.98_{-0}^{+0.01}mm$ ), measuring its size in pixel ( $153 \pm 1px$ ) and converting it knowing the pixel size ( $0.013mm/px$ ) which yields a uncertainty of 1.1%. The reference for the defocusing distance measure is taken when hand positioned item of interest appears sharp at maximum diaphragm opening. By this mean, uncertainty on the defocusing distance is estimated to be  $\sim 1mm$ , which yields  $\sim 1.3\%$ . These two terms are constant over the field therefore only induce a bias on the results. Based on measurement done on relevant reference cases, one could properly adjust the amplification factor  $A$  thus removing the error made on geometrical measurement.

The last term  $J$  in Eq. 10 is the error ratio which may be considered as an estimation of the overall uncertainty of cross-correlation on the signal on the integrated displacement. This term holds both the uncertainty of the cross-correlation algorithm, and the acquisition white noise component. As seen on Fig. 6a, maximum dispersion is held at the center of the reconstruction. On one diameter after the nozzle, reconstructed value in the jet center is supposed to be equal to the  $CO_2$  density, therefore we may consider giving an estimation of  $J$  based on the stochastic oscillations observed on Fig. 6b. Working in steady conditions, a first temporal averaging is done on  $\delta_x$  (i.e. averaging

between the acquisition fields the same way as in Fig. 6 results processing), then the statistics is made along  $y$ . This way one can give a majorant value of  $J$  by a  $J_t$  as follow

$$J \leq \sigma_y \left( \int_{-\frac{L}{2}}^{\frac{L}{2}} |\delta_x \rangle_t dx \right) / \langle \int_{-\frac{L}{2}}^{\frac{L}{2}} |\delta_x \rangle_t dx \rangle_y = J_t \quad (11)$$

Where  $\langle \rangle_t$  is the temporal averaging operator and  $L$  is the field radial dimension. With  $\sigma_y$  being the standard deviation operator in the direction  $y$ , and  $\langle \rangle_y$  being the spatial averaging operator in the vertical direction  $y$ .

In case of unsteady condition when temporal averaging is not possible, a higher majorant,  $J_A$  may be computed. In this case, the statistic should be formed on the ensemble of profiles of each acquisition which yields

$$J \leq J_t \leq \sigma_{y,A} \left( \int_{-\frac{L}{2}}^{\frac{L}{2}} |\delta_x| dx \right) / \langle \int_{-\frac{L}{2}}^{\frac{L}{2}} |\delta_x| dx \rangle_{y,A} = J_A \quad (12)$$

Where  $A$  is the ensemble of a 100 acquisitions. Calculations yields  $J_t \sim 3.1\%$  and  $J_A = 19.1\%$ . This should be compared with the order of the cross-correlation uncertainty which is about 0.1px. Considering that a value of the integration of  $|\delta_x|$  along  $x$  is  $\sim 300$ px, it yields 16.7% of possible PIV uncertainty. Given that PIV intrinsic noise manifests as a white noise, integration and temporal averaging should reduce considerably these value which explains the rather low  $J_t$  value. The total uncertainty on  $I$ , the line of sight integrated density difference, adds up to 5.5%. Doing so, uncertainty is only evaluated before tomography. Tomography adds its own uncertainty in the reconstruction which is quite complex to evaluate. Comparing the oscillations amplitude value (3.5%) with  $J_t$  shows quite values which may indicate that the addition of tomography should be quite low, seemingly in the order of 1%.

Final result uncertainty must take in account the reference temperature and pressure measurement which are used to calculate the ambient gas density and add up a low 1.2%. Uncertainty on measured density is thus estimated to be of 6.7% which is consistent with the 3.5% deviation measured and the 2.3% lower difference of density.

## 6. Application on an electric discharge in air

The electric discharge study is done with a top plug automobile inductive coil (BERU ZSE 041). The electrodes made of tungsten alloy E3® are of 2mm diameter with conic tip of 11.25° half angle and disposed axe aligned, with a gap of 2mm. During the discharge, voltage is recorded with a Tektronix P6015A and intensity with a LeCroy CP031 probe (Fig. 9). Delay is ensured by a pulse and delay generator (DG535, Stanford Research Systems) which synchronizes the camera, the oscilloscope and the coil. For the discharge images are recorded with a defocusing distance of  $l = -36mm$  which yields a higher spatial limitation of  $d_{av} = 0.39mm$ . Because the overall acquisition time is shorter, the laser power is set to maximum (3W) and the intensifier gain is lower to 200 (out of 255). Images are taken 2.5ms after the breakdown, at the end of the glow phase. The heated gas is supposed to be air at ambient composition and pressure for which we apply a semi-perfect behavior. It means that perfect gas law apply and calorific capacity is temperature dependent which is taken as standard Gordon-McBride polynomial form.

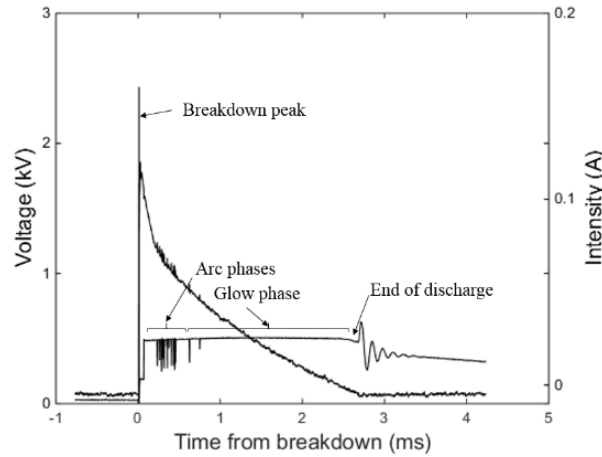


Fig. 1: Electric signal of an electric discharge

Working with ionized gas and considering the Gladstone-Dale constant calculation, one should first estimate electron contribution (Fomin 1998). The work of Maly (Maly 1984) estimates the glow discharge electron density to be of  $N_e \sim 2 \cdot 10^{14} cm^{-3}$ . The contribution to refractive index (Meidanshahi, Madanipour and Shokri 2013) on electron is given by

$$(n - 1)_e \approx -4.46 \cdot 10^{-14} N_e \lambda^2 \quad (13)$$

Therefore  $(n - 1)_e = -2.52 \cdot 10^{-8}$  which should be compared to difference expected with air temperature elevation of at least 700K. Given  $G_{air} = 0.2274 cm^3/g$ , one find  $n_{700K} - n_{293K} = -1.63 \cdot 10^{-4} \gg (n - 1)_e$  thus during glow phase electron contribution is expected to be negligible.

Furthermore, electrons contribution to refractive index is 20.5 times more than the one of ions (Meidanshahi, Madanipour and Shokri 2013). Therefore the refractive index is only supposed to depend on the neutral gas species temperature.

The temperature is directly calculated from density. For enthalpy calculation, one should remember that post-tomography inversion, the field is given in cylindrical coordinates. Calculation is based on the heated mass contained in a cylindrical control volume  $\mathcal{V}$  of 4mm of radius by 4mm wide which includes the phenomena and some non-disturbed area, then with  $C_p$  being the massic calorific capacity at constant pressure,

$$H = \iiint_{\mathcal{V}} (C_p(T) T - C_p(T_{ref}) T_{ref}) \rho dV \quad (14)$$

With  $\rho$  being the heated gas density. Even if tip-tip electrodes configuration is used, the discharge does not appear to be repeatable enough for consistent displacement temporal averaging. Each couple of images will then be processed without averaging which may result in a lower SNR ratio thus in a higher value of  $J$  as of Eq. 12.

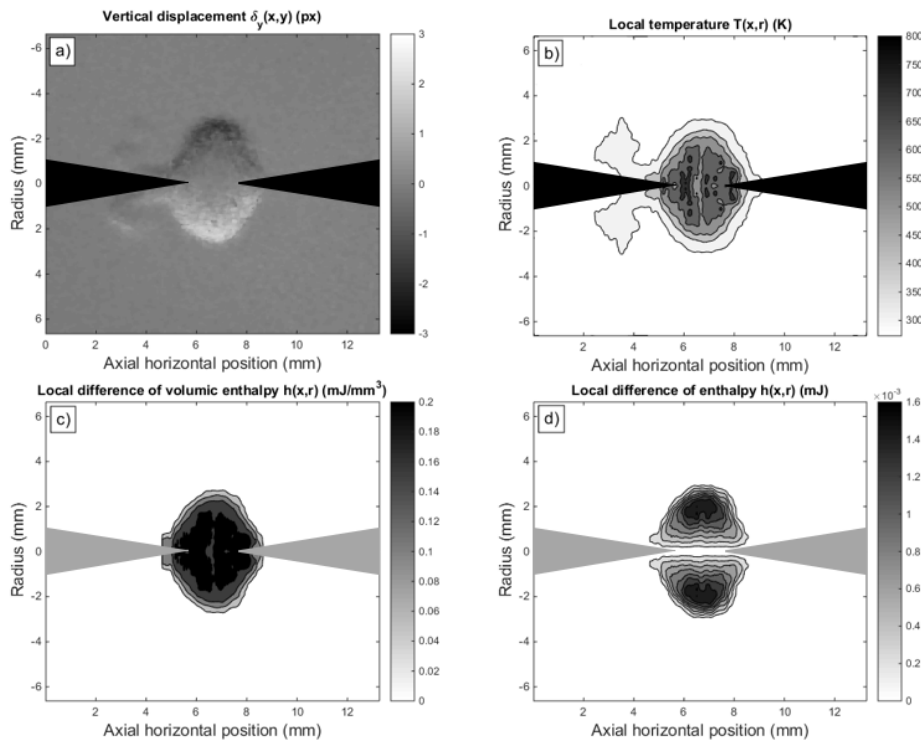


**Fig. 10:** Results in cylindrical referential (attached to the left electrode center) of one images couple through different step of the process of vertical displacement on the electric discharge, from the displacement field (a), to the temperature (iso-100K lines) (b), to the local volumic enthalpy (iso-0.05mJ/mm<sup>3</sup> lines) (c), then to the local difference of enthalpy field (iso-2.10<sup>-5</sup>mJ lines) (d)

The calculation of the displacement is made without any mask, therefore the integration is performed on the electrode's orthogonal displacement component to avoid false vector induced by their shades. However, they are materialized in order to give a spatial reference. On Fig. 8a, one verifies that the displacements are of the same order as the one of the CO<sub>2</sub> jet. Based on 9 images, enthalpy calculation yields  $H = 10.22 \pm 0.47mJ$  which corresponds to a 4.6% deviation.

Although no temporal averaging is done, deviation on the energy calculation is quite low. It seems to confirm the white nature of the noise, despite a  $J_e \sim 19.1\%$  for single shot acquisition on the CO<sub>2</sub> jet, double integration seems to have considerably lowered the dispersion.

Fig. 10d shows that at the end of the process, local enthalpy is not mainly depending on temperature close to the discharge center (i.e. axis). At this time (2.5ms), the kernel temperature is found to be quite low (Fig. 10b) which is a consequence of diffusion and expansion effect of the initial streamer. Considering the rather low temperature (Fig. 10b), volumic enthalpy and massic enthalpy are quite similar (Fig. 10c), enthalpy is only depending on temperature and therefore present the same uncertainty as the jet (Eq. (10)). Local enthalpy is heavily weighted at core by the volume term (which results in a  $1/r$  convolution factor). Therefore enthalpy appears, as presented on Fig. 10d, concentrated in the gradient area, where as showed by Fig. 6a the noise influence is the lowest.

For the calculation of the discharge global efficiency, the electrical energy is calculated at a time  $t$  as the integral

$$E = \int_{t_0}^t VI dt \quad (15)$$

where  $t_0$  is the breakdown starting time, V and I the electrical tension and intensity. Measurements for the 9 acquisition at 2.5ms, right before the discharge stop, yields  $E = 38.36 \pm 1.46mJ$ . This lead to a global efficiency, which can be defined as  $\eta = H/E$ , of  $\eta = 26.67 \pm 1.59\%$ . The results are consistent with the orders and values found in the literature (Saggau 1981) (Teets and Sell 1989) (Verhoeven 2000). Teets (Teets et Sell 1989) with 0.5mm titanium wire in air gives a transfer efficiency of  $\eta = 23 \pm 1\%$ .

## 7. Conclusion

In this paper we presented an experimental method for measurement of axisymmetric field of density based on BOS. The method uses recent BOS development (Meier et Roesgen 2013) with speckle as background (SBOS). We validated the SBOS measurement first on a CO<sub>2</sub> laminar and steady jet with a  $\pm 6.7\%$  estimated maximum uncertainty, close to the  $\pm 2-3\%$  of Elsinga (Elsinga, and al. 2004) and Hargather (Hargather and Settles 2012) and furthermore, corroborated by low experimental dispersion of  $\pm 3.5\%$ . Then the method is extended to enthalpy variation measurement induced by axisymmetric electric discharges. The enthalpy measurement gives satisfying results, with a rather low deviation (4.6%), and are consistent with the ones found in literature (Saggau 1981) (Teets and Sell 1989) (Verhoeven 2000). This successful application of speckle-based BOS for microcalorimetry highlights the quantitative potential and resolution issues of BOS methods applied to highly instationary millimetric-dimension systems. Further work should investigate other discharge instants and configurations.

## Acknowledgements

This work is part of the CAPA research program on Alternative Combustion Mode for air-breathing Propulsion supported by SAFRAN Tech, MBDA France and ANR (National Research Agency).

## References

- Atcheson, Bradley, Wolfgang Heidrich, and Ivo Ihrke. «An evaluation of optical flow algorithms or background oriented schlieren imaging.» *Exp Fluids* Vol. 46, Iss. 3 (2009): pp 467-476.
- Bellenoue, Marc, S. Labuda, B. Ruttun, and Julien Sotton. «Spark plug and corona abilities to ignite stoichiometric and lean methane / air mixtures.» *Combust Sci Technol* Vol. 179, Iss. 3 (2007): pp 447-496.
- Bideau-Mehu, A., Y. Guern, R. Abjean, and A. Johannin-Gilles. «Interferometric determination of the refractive index of carbon dioxide in the ultraviolet region.» *Opt Commun* Vol. 9, Iss. 4 (1973): pp 433-434.
- Dalziel, S., G. Hughes, and B. Sutherland. «Synthetic schlieren.» *Carlomagno GM, editor Proc. Oth international symposium on flow visualization, vol. 62. Sorrento, Italy, 1998.*
- Elsinga, G. E., B. W. van Oudheusden, F. Scarano, and D. W. Watt. «Assessment and application of quantitative schlieren methods: Calibrated Color Schlieren and Background Oriented Schlieren.» *Exp Fluids* Vol. 36, Iss. 2 (2004): pp 309-325.
- Fomin, Nikita A. «Speckle Photography for Fluid Mechanics Measurements.» *Experimental Fluid Mechanics* (Springer), 1998.
- Glassman, Irvin, and Richard A. Yetter. *Combustion, Fourth Edition*. San Diego: Academic Press, 2008.
- Gojani, Ardian B., Burim Kamishi, and Shigeru Obayashi. «Measurement sensitivity and resolution for background oriented schlieren during image recording.» *J Visual-Japan* Vol. 16, Iss. 3 (2013): pp 201-207.
- Grisch, F., G. A. Grandin, D. Messina, and al. «Non-equilibrium kinetic studies of plasma assisted combustion using laser-based diagnostics.» *Z Phys Chem* Vol. 225, Iss. 11-12 (2011): pp 1193-1205.
- Hargather, Michael J., and Gary S. Settles. «A comparison of three quantitative schlieren techniques.» *Opt Laser Eng* Vol. 50, Iss. 1 (2012): pp 8-17.
- Iffa, E. D., A. R. A. Aziz, and A. S. Malik. «Gas Flame Temperature Measurement Using background Oriented Schlieren.» *Journal of Applied Sciences*, Vol. 11, Iss. 9 (2011): pp 1658-1662.
- Keagy, W. R., H. H. Ellis, and W. T. Reid. *Schlieren techniques for the quantitative study of gas mixing*. Columbus, OHIO: Project Rand, 1949.
- Maly, Rudolf. «Spark ignition its physics and effect on the internal combustion engine.» *Dans Fuel Economy*, 91-148. Springer, 1984.

- Meidanshahi, Fatemeh Salimi, Khosro Madanipour, and Babak Shokri. «Measurement of temperature and electrons density distribution of atmospheric arc plasma by moiré deflectometry technique.» *Opt Laser Eng* Vol. 51, Iss. 4 (2013): 382-387.
- Meier, Alexander H., and Thomas Roesgen. «Improved Background oriented schlieren imaging using laser spckle illumination.» *Exp Fluids* Vol. 54, Iss. 6 (2013): 1549.
- Meier, G. E. A. *Hintergrund schlierenmessverfahren*. Deutsche Patentanmeldung, 1999.
- Meier, G. E. A., and L. Venkatakrishnan. «Density measurements using the Background Oriented Schlieren technique.» *Exp Fluids* Vol. 37, Iss. 2 (2004): 237-247.
- Ota, Masanori, Kenta Hamada, and Kazuo Maeno. «Quantitative 3D density measurement of supersonic flow by colored grid background oriented schlieren (CGBOS) technique.» *27th International Congress of the Aeronautical Sciences*. 2010.
- Pancheshnyi, S., D. A. Lacoste, A. Bourdon, and C. O. Laux. «Ignition for propane-air mixtures by a repetitively Pulsed Nanosecond Discharge.» *IEE Trans. On Plasma Science* Vol. 34, Iss. 6 (2006): pp 2478-2487.
- Raffel, M., C. Willert, and J. Kompenhans. *Particle Image Velocimetry-A Practical Guide*. Berlin: Springer, 1998.
- Saggau, B. «Kalorimetrie der drei Entladungsformen des elektrischen Zündfunken.» *Archiv für Elektrotechnik* Vol. 64 (1981): pp 229-235.
- Sveen, J.K. «An introduction to MatPIV v.1.6.1.» *Departement of Mathematics, University of Oslo*, <http://folk.uio.no/jks/matpiv/html/MatPIVtut.pdf>, 2004: Eprint no.2, ISSN 0809-4403.
- Tauer, J., H. Kofler, and E. Wintner. «Laser-initiated ignition.» *Laser & Photon* Vol. 4, Iss. 1 (2010): pp 90-122.
- Teets, Richard E., and Jeffrey A. Sell. «Calorimetry of Ignition Sparks.» *Society of Automotive Engineers*, 1989.
- van Hinsberg, N. P., and T. Rösgen. «Density measurements using near-field background-oriented Schlieren.» *Exp Fluids* Vol. 55, Iss. 4 (2014): 1720.
- Verhoeven, D. «Interferometric spark calorimetry.» *Exp Fluids* Vol. 28, Iss. 1 (2000): pp 86-92.
- Xu, Da. *Thermal and hydrodynamic effects of nanosecond discharges in air and application to plasma-assisted combustion*. Ecole Centrale, 2013.